Humidity, the Dominating Force of Thermal Updrafts

Oliver Predelli
predelli@online.de
Braunschweig, Germany

Ronald Niederhagen
ronald_niederhagen@freenet.de
Marzling, Germany

Abstract

This paper describes the most significant sources of errors and disturbance when measuring temperature and humidity with a glider. Measurement flights have started from different airports in Germany, between April and August of 2018, resulting in a collection of over 90 hours of flight data logs. We show how error correction can be applied to the measurement data. Analysis of the data indicates that core assumptions of the theories of thermals, which have been published for decades cannot be backed up by our measurement data. In contrast we present a revised view of temperature and humidity inside thermals. As a result traditional understanding of temperature distribution and entrainment processes may have to be revised.

Nomenclature

A	surface in m^2
c	specific heat capacity in J/kgK
E	thermal energy in W
g	acceleration of gravity in m/s^2
k	heat-transfer coefficient in W/m^2K
m	mass of the relevant material in kg
$\dot{m}$	air-mass flow in kg/s
T	temperature in K
w	updraft velocity in m/s
w^*	Deardorff's velocity scale
α	heat-transfer coefficient in W/m^2K
θ_v	virtual potential temperature in K
ρ	density of thermal air in kg/m^3
ρ_U	density of environmental air (outside the thermal) in kg/m^3
τ	time constant in s
z_i	depth of the convecting region

Introduction

It is generally assumed that thermals are warmer than the ambient air. Especially in publications intended for a broad readership, this statement can be found. On websites, in magazines, but also in literature for glider pilots. "The main source for updraft in the summer months are warm bubbles of air that rise when the ground is heated by sunlight" [1], writes for example the German Weather Service on its website. Statements, such as "for the dynamics it is crucial to know the temperature difference ΔT between the heated air parcels and the free atmosphere" [2], and "the degree of correlation between temperature and vertical velocity [is significant]" [3] have influenced the collective wisdom of the gliding community over decades. Even the term "thermal" implies heat as the driving influence. But is that really true? Different phenomena make us doubt that an air parcel shall only rise because it is warmer than its ambient air. Some well known phenomena cannot be solely described by a temperature-advance of thermal updraft air compared to the environment:

Fig. 1: The Ventus-2 glider used for environmental measurements.

This article has been reviewed according to the *TS* Fast Track Scheme.

Why are blue thermals predominantly found on the lee side of lakes?; Why is the cloud-base independent of soil properties?; Why can updraft velocity be calculated based on humidity? [4]

One of the best-known formulas for calculating the thermal updraft velocity goes back to James Deardorff, who introduced his convective velocity scale in 1970 [5]:

$$w^* = [\frac{g}{T} z_i \cdot \overline{(wT)_0}]^{\frac{1}{3}} \quad (1)$$

He came up with (1) by folding Monin-Obukhov's description of horizontal winds [6] by 90° upwards. And just like Monin-Obukhov, he has set a few premises, such as "the deviation of density and temperature from the standard values are proportional" and "the Archimedian force only depends on layer temperature and temperature deviation." In other words: Thermals shall be warmer than the environment. Therefore he used the "T" in his equations. Later scientists replaced the temperature T by the virtual potential temperature θ_v, which seems to be much wiser, as buoyancy is driven by density differences [7] and the updraft speed is thus dependent on both, temperature and humidity:

$$w^* = [\frac{g}{\theta_v'} z_i \cdot \overline{w'\theta_v'}]^{\frac{1}{3}} \quad (2)$$

To study the influence of temperature and humidity on thermal updrafts a Ventus-2 glider (Fig. 1) was equipped with environmental sensors. The data acquisition was linked to the on-board aviation instrument data. In-flight measurements were carried out between April and August 2018 in Germany across plains, low mountain range and foothills of the Alps. Weather conditions varied between clear and overcast, between cool spring and hot summer.

Fig. 2: Measurement hardware installed on the Ventus-2 glider.

In-flight measuring equipment

Mobile Devices and Internet of Things (IoT) have triggered a strong investment in sensor technology (Micro-Electro-Mechanical Systems, MEMS) and small portable computer devices (SoC). Over the past decade this investment has led to significant quality improvements as well as cost reduction. It is straight forward to use this equipment in a glider to measure air temperature, humidity and air pressure. Gliders are especially suitable for detailed analysis of thermals because they naturally use thermals flying at low speeds in tight circles.

Nevertheless, measuring air temperature and humidity in flight is nontrivial. There are many sources of errors and mistakes which have to be considered in order to understand the validity of the data. Examples of such errors include the heat capacity of the glider's fuselage which may impact the temperature of the air around it. Or a "dry offset" for humidity sensors which were not designed for high airspeed. Also the result of a water-to-air mixing ratio calculation will be wrong if the temperature measurement was erroneous in the first place. A detailed understanding of the causes to these errors is the basis for developing error correction algorithms. They can be used to eliminate errors in a post-process after the data acquisition. Ignoring these erroneous effects may result in faulty interpretation of the data. Several attempts of former in-flight data acquisition suffer from that.

A sensor of type BME280 from Bosch Sensortec [8] is used to sample humidity, pressure and temperature data. The sensor is operated from a dedicated micro controller which records the data from the BME280 together with a GPS-based timestamp (Fig 2). The data from the glider's flight and navigation instruments are recorded in a separate unit also together with a GPS-based timestamp. Both units' sample rate is 2 Hz. After the flight the two recorded data streams are synchronized, by means of the GPS-based timestamps, merged together and the result is written to a CSV file containing one data vector for every half second. Among, other data the data vector includes humidity, temperature, as well as static pressure, impact air pressure, GPS-fix, course, TE-vario and airspeed.

It is important to pick the optimal position on the glider for the environmental sensors. Unpredictable influences must be avoided or at least minimized and systematic influences must be modeled to allow for data correction in the post-process. Systematic influences include variation in airspeed, influences of parasitic heat capacity upstream or around the sensor, or heat radiation from the sun. Unpredictable influences include turbulent airflow around the sensor or yawing of the glider which changes the airflow around the sensor as the alignment changes between the glider's roll axis and the glider's motion vector. Thus the sensor may be exposed to either fresh air or air which has flown over the surface of the glider.

For the data acquisition of this publication, the sensor was positioned inside the ventilation channel to the cockpit of the glider. Thus it is protected from direct sunlight and the misalignment of the glider's roll axis has nearly no effect.

Temperature correction

Basic considerations

The result of the effects mentioned above is that the measured temperature suffers from a time lag relative to the temperature of interest. On falling air temperature (during ascend) the sensor

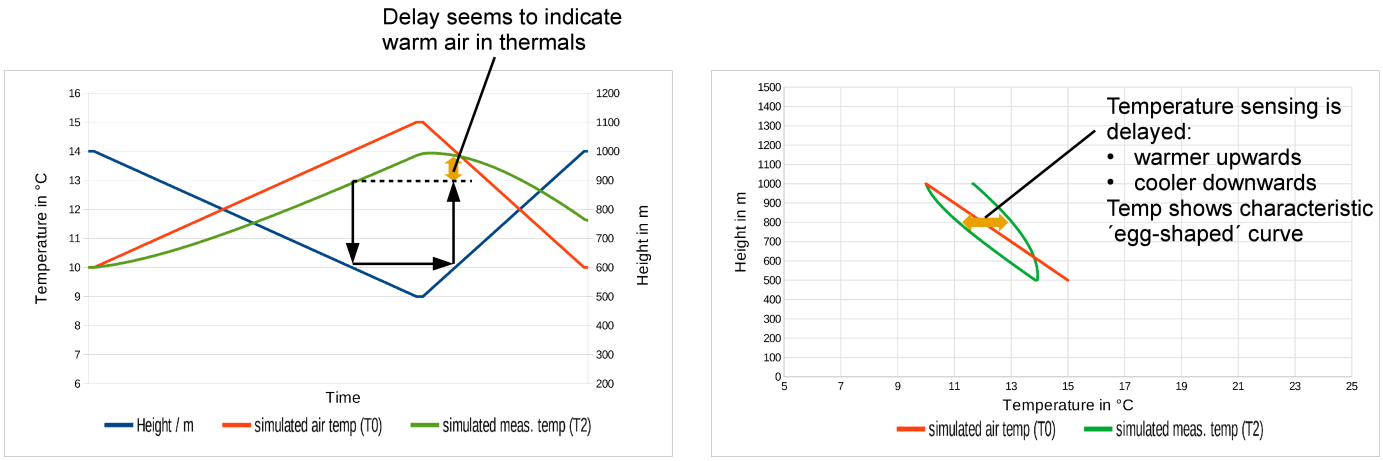

Fig. 3: The uncorrected raw temperature sensor signal indicates a faulty temperature advance of a thermal.

reads a slightly warmer temperature. Whereas in rising air temperature (during descend) the reading is slightly colder. Plotting altitude over temperature exhibits a more or less distinct loop form, very much resembling a hysteresis curve (Fig. 3).

There are some older publications which interpret this loop form as a temperature difference between the thermal and the ambient air with increased potential temperature during ascent and reduced potential temperature during descent. One example where the loop form becomes apparent is during the tow phase. During that phase the tow plane pulls the glider to the release point. Typically this is an ascent outside of thermals. There should be no increase of the potential temperature under these conditions. If potential temperature increased, a time lag was influencing the temperature measurement.

The most noticeable influence on the sensor's operation is caused by the presence of heat capacity upstream from the sensor and the heat capacity of the sensor package and fixture itself (Fig. 4).

The ambient air with its temperature T_0 heats the aircraft and the sensing equipment. There is always a heat transfer $\dot{Q}_1$ from the environment to the aircraft and its equipment. At the same time, there is always a heat transfer $\dot{Q}_2$ from the aircraft and the sensing equipment back into the measurement air: On its way to the temperature sensor, the measurement air sweeps along the surface of the aircraft and through the measuring equipment. The aircraft's surface temperature T_1 follows the ambient temperature T_0 time-delayed with a first order low-pass filter. This delay is caused by the heat capacity of the aircraft's fuselage. Part of the surface temperature T_1 is transferred to the measurement air. It can be shown that the heat transfer from the aircraft back into the measurement air depends on the temperature difference between the aircraft and the environmental air flowing into the measurement equipment. This heat transfer is represented by the factor f in the block diagram Fig. 5, with $0 \leq f \leq 1$. Depending on whether the surface temperature is warmer or colder than the ambient temperature, the measurement air is warmed or cooled. T_2 represents the measured air temperature at the sensor position.

T_2 depends on the measuring setup how strong the temperature change of the measurement air is. However, an influence always takes place, at least because of the housing of the probe.

Physical description of the measuring system

In Fig. 4 we show a conceptual picture of the measuring device in proximity with the parts of the fuselage of the glider. In this case the temperature T_1 of the relevant parts of the glider,

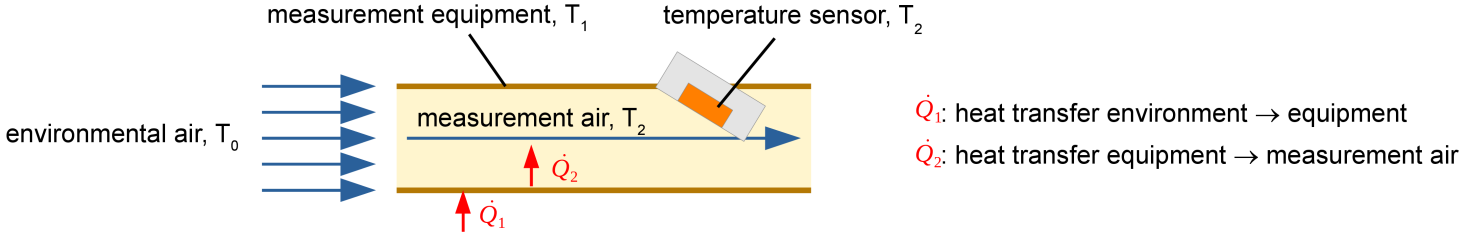

Fig. 4: The influence of heat transfer on the measured air temperature.

the incoming ambient air temperature T_0 and the temperature T_2 at the sensor position are functionally related by

$$\frac{T_2 - T_1}{T_0 - T_1} = exp\left(-\frac{\alpha \cdot A}{\dot{m} \cdot c_p}\right), \tag{3}$$

as developed in [9].

The parameters α (heat-transfer coefficient in W/m^2K), A (surface of the air-flow channel in m^2), $\dot{m}$ (air-mass flow in kg/s) and c_p (specific heat capacity of air in J/kgK) are assumed to be sufficiently constant. Therefore the exponential function can be simplified to the constant (1-f) with $0 \leq f \leq 1$. The value for f must later be determined by a measurement data analysis. Eg.(3) can thus be transformed into

$$T_2 = T_1 \cdot f + T_0 \cdot (1 - f) \tag{4}$$

Equating the definition of the heat flow

$$\dot{Q} = k \cdot A \cdot (T_0 - T_1) \tag{5}$$

with the definition of the heat capacity, here derived by time,

$$\dot{Q} = c \cdot m \cdot \dot{T}_1 \tag{6}$$

results in a differential equation of the first order, which describes the temperature profile T_1 of aircraft and equipment material as a function of the ambient air temperature T_0:

$$\frac{c \cdot m}{k \cdot A} \cdot \dot{T}_1 + T_1 = T_0 \tag{7}$$

T_1 follows T_0 time-delayed like a first-order, low-pass filter with the time constant $\tau = (c \cdot m)/(k \cdot A)$.

As in (3) the parameters c (specific heat capacity of aircraft and measuring equipment), m (mass of the relevant material), k (heat-transfer coefficient) and A (relevant surface of the aircraft) are sufficiently constant so that the time constant τ also remains constant over the various operating states and altitudes of the aircraft. Also τ must later be determined by a measurement data analysis.

Fig 5 shows the relationship between the environmental temperature T_0 in front of the aircraft's nose, the body temperature T_1 and the temperature T_2 at the sensor position in a block diagram, based on (4) and (7).

Correction algorithm

The measuring equipment records T_2 with a fixed sample rate of $\Delta t = 0.5$ sec. Therefore the block diagram in Fig. 5 can be merged in a simple difference equation, with $k-1$ and k representing the discrete samples of the temperature values

$$\begin{aligned} T_{2(k)} &= T_{0(k)} + f \cdot (T_{1(k)} - T_{0(k)}), \\ \text{with } T_{1(k)} &= T_{1(k-1)} + \frac{\Delta t}{\tau + \Delta t} \cdot (T_{0(k)} - T_{1(k-1)}) \end{aligned} \tag{8}$$

In our case a time constant τ for the low-pass filter and f have been determined in lab experiments and have been verified by correlation of nearly 100 hours of flight data records.

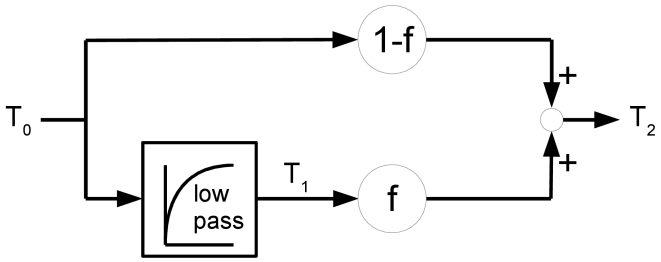

Fig. 5: Block diagram to describe the influence of heat transfer and heat capacity on the measured air temperature with T0: environmental air temperature in front of the aircraft; T_1: temperature of the equipment; T_2: air temperature at the sensor position.

Not shown in Fig. 5 is a second time constant of approximately 5 seconds reflecting the package and the fixture of the BME280 sensor itself. However, it turns out that the second time constant can be safely ignored as it has only a minor impact on the calculation. This simplifies the correction algorithm.

The recorded data is post-processed such that the temperature T_0 in the undisturbed air immediately in front of the glider's nose is available for subsequent calculation by a simple mathematical inversion of (8). It is important to note that the applied data correction for T_2 does not depend on the altitude nor does it imply any form of dry-adiabatic lapse rate.

The temperature error can be estimated by comparing a simulated measurement temperature with the actual measurement temperature (Fig. 6). Based on the height data (in blue) a theoretical temperature T_0 (in red) is simulated in which a dry-adiabatic temperature gradient is considered. The parameters τ and f are tuned to achieve maximum correlation between simulation and measurement. By doing this with different measurements, constant values for τ and f can be identified. These two values are the same for all measurements on all days and for all flights.

The error band of the calculated temperature has been found to lie within a range of less than $\pm 0,1$ K of the measured value. This also proves the correctness of the block diagram in Fig. 5 and the expected physical behavior.

Now equation 8 is inverted. If the measured temperature T_2 is used as the input data for the inverted algorithm, the corresponding real air temperature T_0 in front of the aircraft's nose is the calculated result.

If the measured temperature data T_2 (the uncorrected raw data of the sensor) is plotted in a diagram with the height above the temperature, a quite characteristic egg-shaped curve results. When climbing, the glider can not cool to the temperature of the ambient air. The glider warms the measurement thus the measurement temperature seems to be warmer than the ambient temperature. When descending, it is the other way around. If one compares the temperatures during the climb and the descent at the same altitude, one could mistakenly conclude that there is

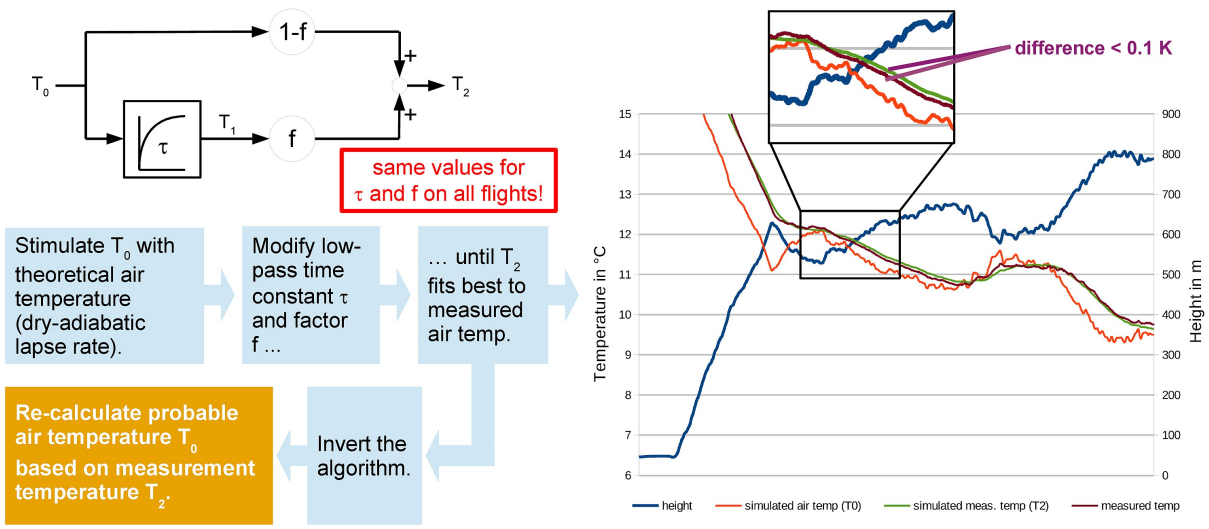

Fig. 6: Parameter identification of the algorithm for the temperature correction.

a temperature advantage of the thermals compared to the ambient air as already explained in Fig. 3. This underlines the need for the correction method described above.

Humidity correction

The in-flight measurements show that the humidity sensor of the BME280 exhibits a "dry offset". The relative humidity is always too low resulting in a calculated dew point temperature which is ~ 2.5 °C lower than expected. This dry offset only can be observed in flight. When standing still on the ground or in the lab the dew point values correspond to the values published by the German Weather Service (DWD) for that place and time. We assume the dry offset has to do with the speed at which the air passes by the sensor. The BME280 may not have been designed for such conditions although the data sheet is not explicit about that.

One possible and plausible explanation for the dry offset behavior under those conditions can be related to the measurement principle of the sensor. A thin layer of water builds on the surface of such solid-state capacitive moisture sensors [10]. This water film is a few molecule diameters thick and is caused by adsorption. The thickness of the adsorbed water film depends on the relative humidity and the temperature of the measured air and represents the measurement principle of this sensor type.

As pointed out in [10], the strong air flow around the sensor may cause a reduction in thickness of the adsorbed water film. This leads to the afore mentioned dry offset and the lower than expected humidity values from the sensor (Fig. 7).

Considering Van-Der-Waals-Forces we correct the thickness of the water layer thus correcting the relative humidity values. As with the temperature correction, also the humidity correction is independent of the particular flight or any other parameter, so that the same algorithm can be applied to correct all acquired data.

Results

First thermal after take-off

Fig. 8 shows the results of a flight on May 14, 2018. The plot uses a format which is widely used for thermodynamic diagrams. The black line shows the uncorrected temperature values exhibiting the afore mentioned loop form (T_2 in Fig. 4). The red curve on the right shows the corrected temperature (T_0 in Fig. 4). The blue curve shows the dew-point temperature. Letters denote significant time points during the flight which include: the end of the tow phase after takeoff, searching and circling in the first thermal, cruising to the next thermal. The embedded graphic displays the different phases of the flight, plus an additional

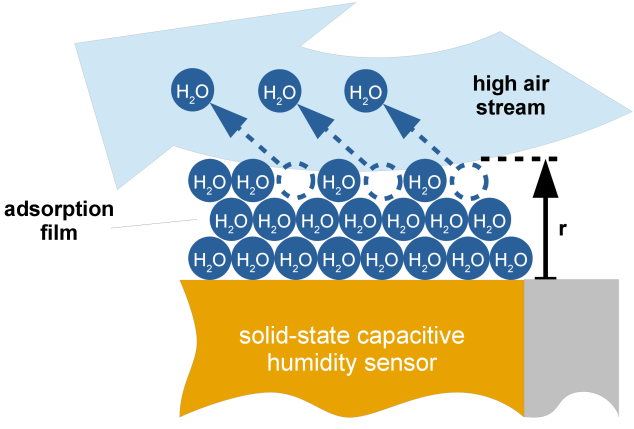

Fig. 7: Assumed cause of the dry offset and the lower than expected values from the humidity sensor.

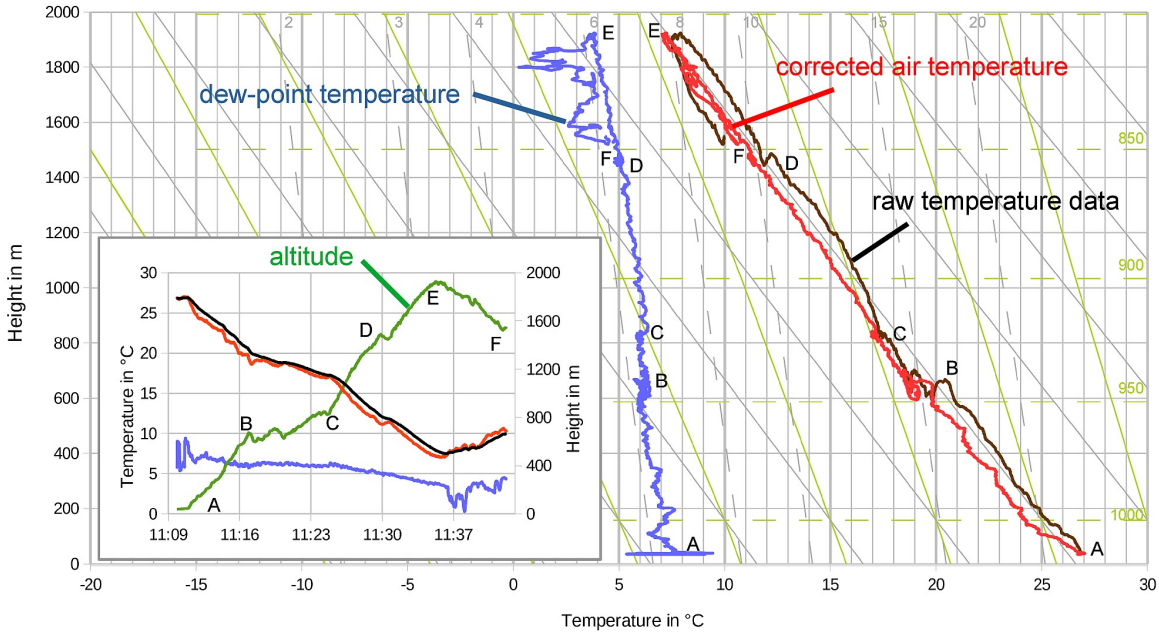

Fig. 8: Temperature and dew-point temperature during a flight on May 14, 2018. A: takeoff; B: release; C: entering 1st thermal; D: entering 2nd thermal; E: leaving thermal; F: entering 3rd thermal

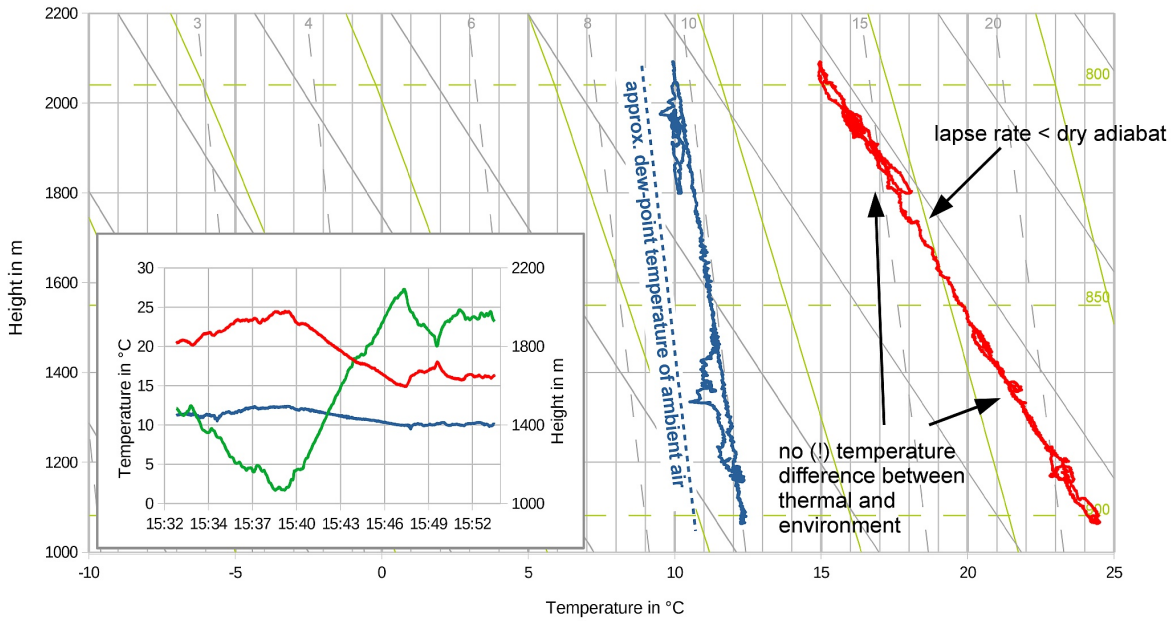

Fig. 9: Temperature and dew-point temperature during a flight on July 25, 2018.

curve showing the altitude above takeoff level.

It can be seen in Fig. 8 that the corrected temperature curve aligns on a common line for all phases of the flight. Thus, there is no measurable temperature difference between the thermal and the ambient air. Furthermore, it is obvious that the dew point temperature correlates nicely with the line of constant mixing ratio during the ascent inside the thermal (section C-D-E in Fig. 8). The mixing ratio is almost independent of the altitude which lets us conclude that there was no significant mix with (drier) ambient air. Any form of entrainment or dilution would have lead to a change of the mixing ratio with increasing altitude.

During the cruising phase we measure mostly the humidity

of the ambient air, clearly drier than inside the thermal (section E-F). But, also during that phase of the flight, we experience patches of humid air caused by small thermals in between the main thermals which the pilot decided to use. During the tow phase and at the release of the tow-rope (section A-B) we experience temperature spikes. This is probably related to the exhaust from the tow plane's combustion engine.

Another typical thermal updraft

Fig. 9 shows another typical updraft, flown on July 25, 2018. Before entering the updraft, inside the updraft and after leaving the updraft, the air temperature in the respective height is always the same. This updraft is not warmer than the ambient air.

Within the thermal, the dew point temperature follows the line of equal mixing ratio. Before entering the thermal and after leaving the thermal, the air is clearly drier. It can be assumed that the dew-point temperature of the ambient air is approximately on the dotted blue line. That is, the air in the updraft has a lower density than the ambient air because it contains more humidity, not because it is warmer. The driving force behind the buoyancy is the moisture difference, not the temperature difference!

A closer look at the lapse rate of the thermal shows that it is slightly warmer than the dry adiabat. The red temperature curve is not parallel to the gray dry adiabats. This is another more indirect proof that the temperature inside the updraft corresponds to the environment.

Lateral entrainment

Below 1300 m the dew-point temperature in Fig. 10 follows almost constantly a mixing ratio of approximately 8.5 g/kg. In fact the humidity inside the thermal becomes a little drier with increasing height. The mixing ratio moves a little to the left and reaches 8 g/kg in 1800 m. This change indicates lateral entrainment at the edges of the updraft. So lateral entrainment seems to be relatively small in thermal updrafts.

Circling up to cloud base

The measurement data are sufficiently detailed that they also allow a look at some interesting details. Fig. 11 shows a flight up to the cloud base, where the glider flew in an area of incipient condensation. Good to see is the cooling of the ambient air under the cloud after the aircraft has left the updraft stream. This is because water droplets fall out of the cloud, evaporate and thereby cool the air.

In close vicinity to the updraft air flow, downdrafts are noticeable. They are relatively dry. These downdrafts are created by entrainment on cloud top, sink through the entire cloud and exit out of the cloud base [11]. Of course, these downdrafts, like the updrafts, have the same temperature as the ambient air. They are neither warmer nor colder. They only fall because they are drier and, thus, have a higher density than the ambient air.

Blue thermals with different strength and estimated mixing at ground level

Two consecutive blue thermals A and B in a distance of approximately 6 km are analyzed in Fig. 12. Both updrafts have the same temperature. But it can be seen that the stronger thermal with 2.3 m/s is moister compared to the ambient air than the weaker neighbor with only 1.2 m/s.

We only have few data points for thermals at low altitude

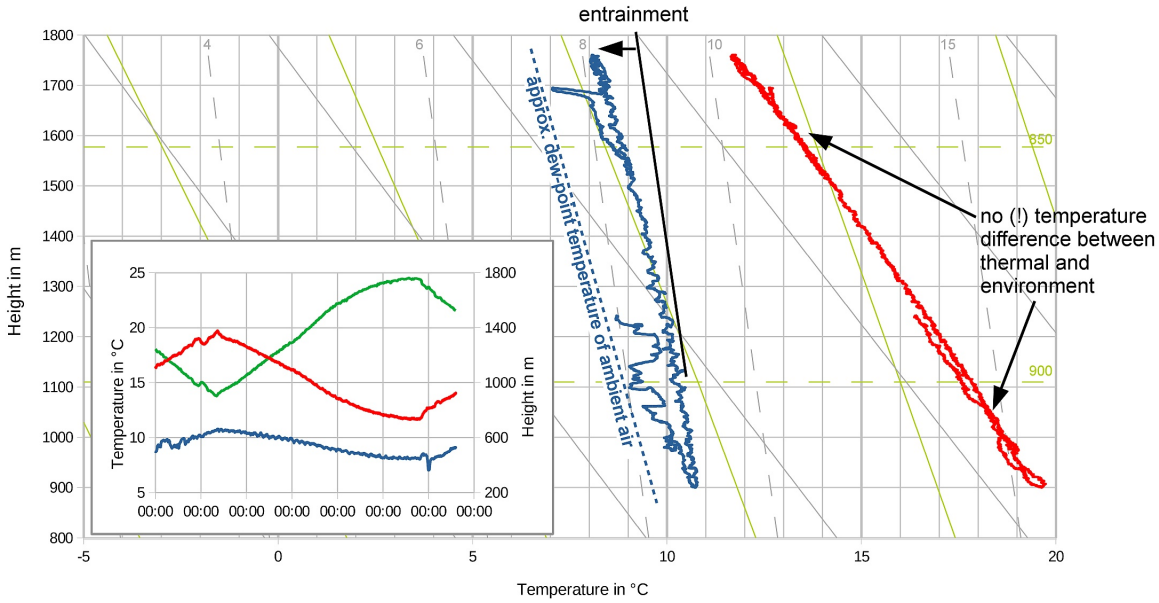

Fig. 10: Temperature and dew-point temperature during a flight on May 26, 2018 with typical lateral entrainment.

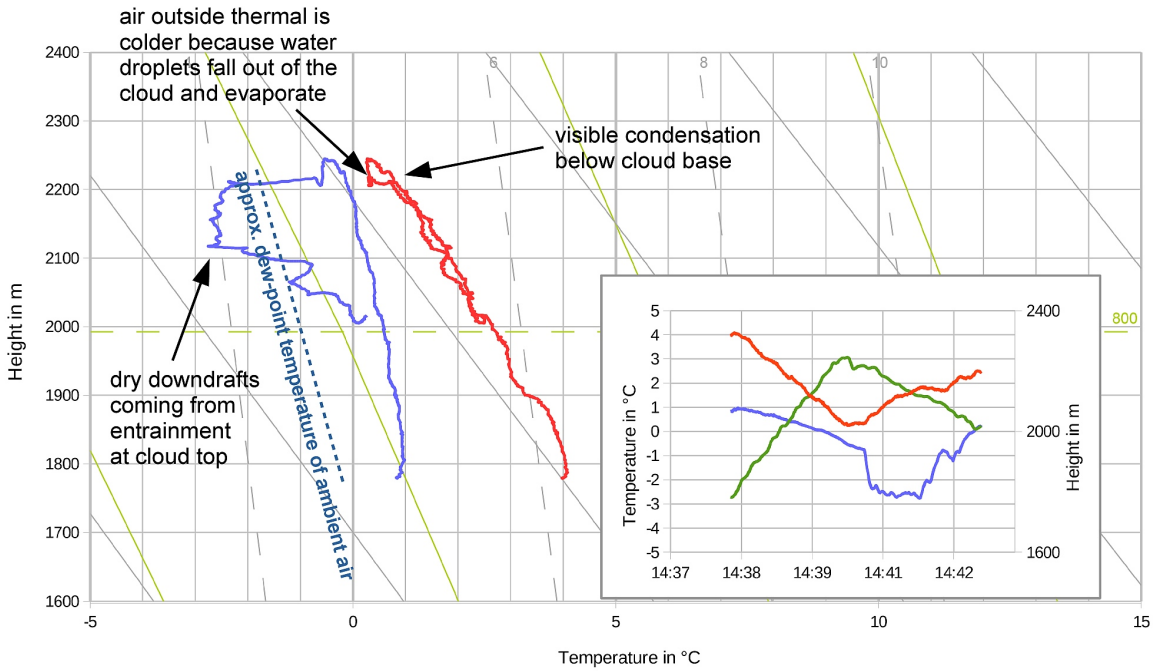

Fig. 11: Temperature and dew-point temperature at cloud base during a flight on August 26, 2018.

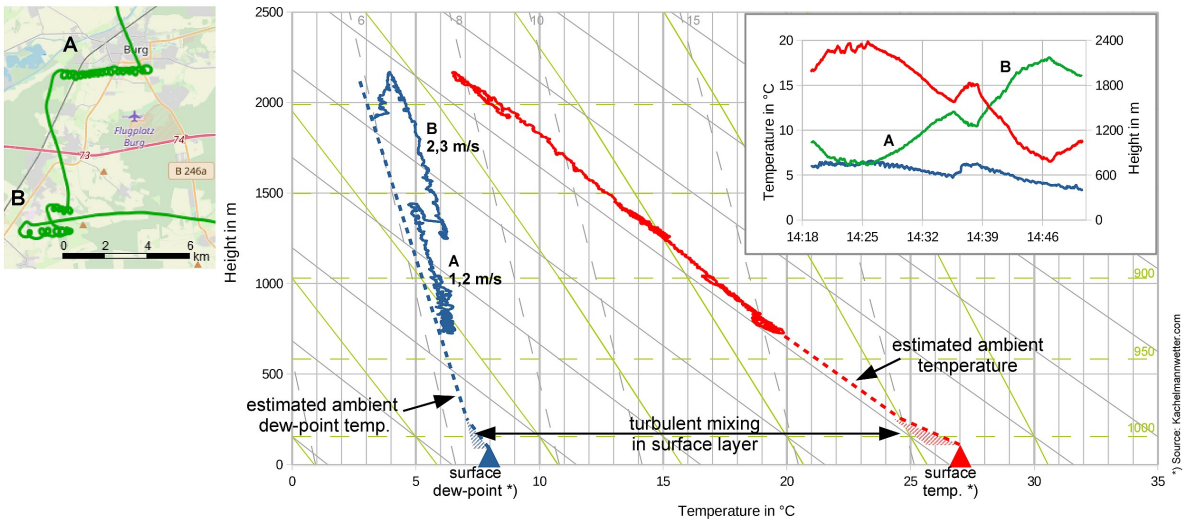

Fig. 12: Two consecutive blue thermals A and B with different updraft velocities during a flight on May 13, 2018.

(<500m GND). Hence we can not be really sure what the temperature curves look like between the surface layer and the first few hundred meters height. However, we believe there is a positive temperature difference which is needed to get the thermal off the ground. Down there and only down there thermals are really warmer than the environment. As the air rises, this temperature difference decreases by the ascend itself as well as by mixing with cooler ambient air. As the formation of an updraft is connected with horizontal winds near the ground, intense turbulent mixing will soon reduce any temperature advance. Thus there seems to be higher entrainment close to the ground compared to higher altitudes.

Updraft velocity based on humidity differences

Fig. 12 shows the climb rates achieved by the glider in two neighboring thermals. The thermals differ in moisture, but their temperature being the same as the ambient temperature. A short study shall analyze whether the different climb rates also can be

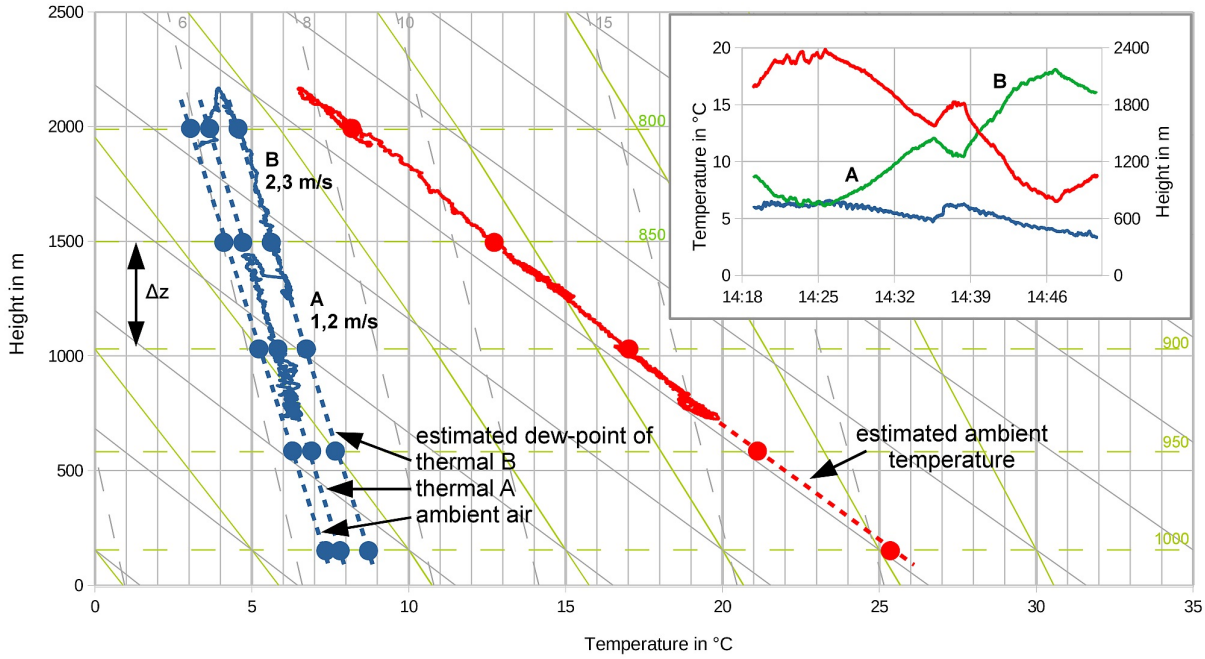

Fig. 13: Parameters for the updraft velocity calculation.

determined mathematically.

Liechti and Neininger [2] present a simplified algorithm, which is used by the German Weather Service in the thermal forecasting software "ALPTHERM" for the calculation of updraft velocity . It is based on the Euler equations of fluid dynamics, from which, after a few transformations, the thermal energy E per air parcel mass m_p is calculated for discrete height layers:

$$\frac{dE}{m_p} = g \cdot \Delta z \cdot \left(\frac{\frac{\rho_U[n+1]}{\rho[n+1]} + \frac{\rho_U[n]}{\rho[n]}}{2} - 1 \right) \tag{9}$$

The height layers lying one above the other have the thickness Δz. The density of the thermal air is ρ, the density of the ambient air is ρ_U. The indices n and $n+1$ identify the associated values on the bottom and top of the respective height layer in order to obtain an average value for dE/m_p using (9). The separate mean values are then added up to the total specific energy per air parcel:

$$\frac{E}{m} = \sum \left(\frac{dE}{m_p} \right)_{n \to n+1} \tag{10}$$

and from this the updraft velocity is calculated:

$$w = \sqrt{2 \cdot \frac{E}{m}} \tag{11}$$

ALPTHERM then makes further corrections to the updraft velocity in order to take entrainment or the wind influence into account. These additional improvements to the simulation result are not considered here for reasons of simplification.

Fig. 13 and Table 1 show the application of (9) to (11) to the two neighboring thermals of the flight from May 13, 2018 in Fig 12. Unlike in ALPTHERM, layer thicknesses of Δz = 100 m are not used here, but layers of approximately 500 m, which are based on the air pressure difference of 50 hPa. Temperature and dew point temperature values are taken from the temperatures in Fig. 13. The dew point temperatures of the two thermals were extrapolated linearly over the relevant altitude range. The associated air densities ρ and ρ_U are calculated from the moisture-dependent different dew point temperatures, but with the same air temperature for ambient air and thermal air with the aid of [12]. The updraft velocity of the respective thermal then is determined from the equations above.

As shown in Table 1, it is striking that the calculated climb rates are comparable with the climb rates of the glider. Due to the simplified climb rate calculation (height steps of approximately 500 m, no entrainment, no wind influence, no consideration of the effects in the immediate vicinity of the ground) there is always a certain deviation between the theoretical values and the values flown. Also the self-sinking of the glider, which is about 0.5 m/s in slow circular flight, must be added to the measured climb rates. However, it becomes clear that even in this calculation the updraft velocity in thermal B is greater than in thermal A, and the difference between the two climb rates is in the same order of magnitude as the measured flight data. Here too is confirmed that the updraft velocity depends on the moisture inside the thermal, whereas a different temperature is not necessary in the mathematical calculation to explain the difference in climb rates.

Thermal A						
z in m	air press. in hPa	ρ in kg/m^3	ρ_U in kg/m^3	dE/m_p in m^2/s^2	calculated updraft in m/s	measured updraft in m/s
2000	800	0,98771	0,98758	0,846		
1500	850	1,03179	1,03157	0,796		
1040	900	1,07648	1,07633	0,616	2,4	1,2
580	950	1,12082	1,12067	0,546		
170	1000	1,16196	1,1618			
Thermal B						
z in m	air press. in hPa	ρ in kg/m^3	ρ_U in kg/m^3	dE/m_p in m^2/s^2	calculated updraft in m/s	measured updraft in m/s
2000	800	0,98771	0,98732	2,158		
1500	850	1,03179	1,03129	2,038		
1040	900	1,07648	1,07603	1,870	3,9	2,3
580	950	1,12082	1,12036	1,657		
170	1000	1,16196	1,16148			

Table 1: Climb rate calculation and comparison with flight data.

Conclusions

Difference in air-density is the driving force behind thermals. Difference in temperature and humidity is the primary cause of this buoyancy. Extensive measurements over Germany in the summer of 2018 show that humidity is the dominating moving force of the thermals, at least in the upper three quarters between ground and cloud base. In order to recognize this dominance, it is essential either to prevent interfering influences on the temperature measurement or to compensate the measured data mathematically. A faulty temperature measurement can lead to the incorrect conclusion that the drive of the thermals is attributed to a, actually not existing, temperature difference. Furthermore, the algorithms for calculating the thermal strength should also take into account the moisture difference and not rely solely on temperature difference. Future measurements will investigate more closely the lower realms where temperature difference is expected to dominate the convective updraft. As the temperature difference disappears within a few hundred meters due to lateral entrainment and mixing, a thermal's ascent is non-adiabatic.

Maybe another word for convective updrafts should be used: They are obviously more a "moistal" than a "thermal".

References

[1] "`https://www.dwd.de/EN`," *Deutscher Wetterdienst*, follow path: RESEARCH/Weather forecasting/Meteorological algorithms and applications/Applications for Aviation Weather Forecasts/Weather forecasts for gliding, download 08.01.2019.

[2] O. Liechti, B. Neininger, "ALPTHERM - A PC-based Model for Atmospheric Convection over complex Topography," *Technical Soaring*, Vol. 18, No. 3, 1994, pp. 73–78.

[3] Milford, J. R., "Some Statistics of Thermals Observed by a Powered Sailplane," *XVI OSTIV Congress*, 1978.

[4] Predelli, O., "Thermikprognose mit Temps," *segelfliegen*, , No. 3, 2017, pp. 24–28.

[5] Deardorff, J., "Preliminary Results from Numerical Integrations of the Unstable Planetary Boundary Layer," *Journal of the Atmospheric Sciences*, Vol. 27, 1970, pp. 1209–1211.

[6] A. S. Monin, A. M. O., "Basic laws of turbulent mixing in the surface layer of the atmosphere," *Tr. Akad. Nauk SSSR Geophiz. Inst 24(151)*, 1954, pp. 163–187.

[7] Stull, R. B., *An Introduction to Boundary Layer Meteorology*, Kluwer Academic Publishers, 1988, p. 355.

[8] "Bosch Sensortec GmbH: BME280 Combined humidity and pressure sensor," *Final data sheet*, 2016, Revision 1.3.

[9] K.-H. Grote, J. F., *Taschenbuch für den Maschinenbau*, Springer, 23rd ed., 2011, p.K46.

[10] Anderson, P. S., "Mechanism for the Behavior of Hydroactive Materials Used in Humidity Sensors," *Journal of Atmospheric and Oceanic Technology*, Vol. 12, 1995, pp. 662–667.

[11] Predelli, O., "What goes up must come down," *segelfliegen*, No. 3, 2018, pp. 38–47.

[12] "`https://www.omnicalculator.com/physics/air-density`," .